External surface temperature measurements for the heat transfer analysis of internally heated cylindrical clad-tubes subjected to external forced convection bulk water coolant thermal-hydraulic conditions

K. Govinder, J.F.M. Slabber and J.P. Meyer

Department of Mechanical and Aeronautical Engineering, University of Pretoria, Pretoria 0002, South Africa

*Corresponding author. chris.govinder@up.ac.za

Highlights

• External surface temperature measuring issues during flow boiling is discussed.

• An innovative method is presented to measure the external surface temperature.

• Relatively good agreement between experimental and predicted values were achieved.

• External flow boiling heat transfer can be analysed with generalised correlations.

Abstract

In a worldwide pursuit for more Accident Tolerant nuclear Fuel (ATF), the quest to obtain and certify alternative nuclear fuel cladding tubes for light-water nuclear power reactors is still a key challenge. One of the facets in this program to develop more ATF is the heat transfer evaluation between the various proposed clad tubes manufactured from suitable replacement materials and the current zirconium-alloy based clad tubes used in nuclear power reactors. For the heat transfer analysis, the accurate measurement of the temperature on the heat transfer surface of heated tubes to be tested was one of the important objectives for the effective analysis of the heat transfer characteristics to the water coolant. After extensive investigations, a suitable technique was developed and validated against recognised forced convection heat transfer correlations. The results showed that this technique was well suited for external forced convection heat transfer studies from heated surfaces exposed to forced convection water coolants.

Keywords
External flow boiling; surface temperature measurement; SiC; ATF; fuel clad-tubes

Nomenclature

List of Symbols

Bo

Boiling number, $\dot{q}/Gh_{fg}$

Co

Convection coefficient, $(x/(1-x))^{0.8}(\rho_g/\rho_l)^{0.5}$

C_p, kJ/kg.°C

Specific heat

E

Enhancement factor (as used in Gungor and Winterton, 1985)

F

Enhancement factor (as used in Chen, 1966, Gungor and Winterton, 1987, Liu and Winterton, 1991)

F_{fl}

Fluid dependant parameter

Fr

Froude number, $G^2/\rho_l^2 gD$

G, kg/m².s

Mass flux, $\rho V/A_s$

H, kW/m².°C

Heat transfer coefficient

h_{fg}, kJ/kg

Enthalpy of vaporization

h_l, kJ/kg

heat transfer coefficient for liquid only phase

K, W/m.°C

Thermal conductivity

M, kg/kmol

Molar mass

Pr

Prandtl number

p_r

Reduced pressure, P_{abs}/P_{crit}

$\dot{q}$, kW/m²
: Heat flux

Re_l
: Liquid Reynolds number, GD/μ_L

S
: Suppression factor

T, °C
: Temperature

T_f, °C
: Film or interface temperature

ΔT, °C
: Temperature difference

ΔT_{ex}, °C
: Superheat or excess temperature

x, %
: Vapour quality

X_{tt}
: Lockhart-Martinelli parameter

Greek Symbols

μ, kg/m.s
: Dynamic viscosity

ρ, kg/m³
: Density

σ, N/m
: Surface tension

ψ
: Heat Transfer Enhancement Factor (as used in Shah, 1977)

List of Subscripts

b
: Bulk coolant

ex
: Wall superheat or excess temperature

fc
: Single phase forced convection

in
: Inlet; input

l
: liquid; liquid only condition

meas
: Measured value

pool
: Pool boiling condition

pred
: Predicted value

s; *sat*
: Saturated

TP
: Two-phase condition

v
: vapour

w
: Wall (clad-tube heat transfer surface)

List of Abbreviations

CHF
: Critical heat flux

FDNB
: Fully developed nucleate boiling

HTC
: Heat transfer coefficient

HTR
: High-temperature reactor

LWR
: Light water reactor

ONB
: Onset of nucleate boiling

OSV
: Onset of significant void

PNB
: Partial nucleate boiling

SiC
: Silicon carbide

UP-THFC
: University of Pretoria - Thermal-Hydraulic Flow-loop Cell

Zr-4
: Zircaloy-4®

1. Introduction

There are relatively few materials in existence that is adequately suited to perform the very important functions of nuclear fuel cladding (Lamarsh and Barata, 2001, Anglart, 2011). In particular, the fuel cladding must be stable under irradiation conditions whilst also possessing other important material characteristics such as small neutron absorption cross-section, high corrosion resistance, and reasonably long-term structural stability whilst exposed to neutron irradiation. Metallic zirconium-alloy based materials have for many years fulfilled this function within most light-water nuclear power reactors (LWRs) but, unfortunately, these zirconium-based materials also have some operational shortcomings and limitations (McMinn et al., 1998, Voglewede, 2012, Buongiorno, 2011). One major shortcoming, as is the case with most materials, is the exothermic oxidation reaction of the zirconium-alloy fuel cladding in the presence of high temperatures and steam which subsequently has a huge potential for hydrogen generation (Buongiorno, 2011, Accident-Tolerant Fuel Valuation: Safety and Economic Benefits (Revision 1) 300, 2019). For example, this condition could arise if, for whatever reason possible, there is a total loss of coolant flow through the reactor causing the dry out and evaporation of the water inventory in the reactor vessel. This type of condition could lead to the eventual exposure of the very hot fuel cladding to the subsequent steam formation in the vessel (Gurgen and Shirvan, 2018). The uncontrolled generation and accumulation of hydrogen within a nuclear reactor is highly undesirable which could lead to explosions within the reactor containments – as was witnessed in the Fukushima-Daichi incident in 2011 (Fukushima Daiichi Accident, 2020). Other shortcomings of the zirconium-alloy based nuclear fuel cladding include amongst others – hydration effects from neutron irradiation in a typical core environment that leads to the swelling of the metallic structure, and the embrittlement of the metallic structure when exposed to extreme heat sources such as decay heat produced by fission products that could result in the degradation of the cladding and potentially cause the uncontrolled release of fission products (Lamarsh and Barata, 2001). Due to this, the total lifespan of most zirconium-alloy based nuclear fuel cladding is limited to about five years on average. Currently, most Zircaloy® clad fuel is replaced in around 18-month cycles due to the consumption of the fissile material, build-up of fission products and to guard against potential structural failure of the cladding (Nechaev, 1993).

Silicon Carbide (SiC) have been investigated and proposed as one such potential cladding replacement material (Lee et al., 2014, Carpenter et al., 2007). SiC yielded satisfactory results after being exposed to extensive irradiation in experimental programs involving amongst others testing as a cladding material in High-Temperature Reactors (HTR) (Nishio, 2004, Feinroth et al., 2009, Sukjai et al., 2014). The heat transfer characteristics of the SiC to water coolants are still under investigation. In contributing to this international research, a program was initiated at the University of Pretoria to conduct heat transfer tests on the SiC and to compare it with similar tests on typical Zircaloy-4® (Zr-4) clad-tube specimens.

The clad-tube surface temperature T_w was one of the major parameters to be measured in the heat transfer tests. However, efforts to measure this temperature proved to be quite difficult. Information regarding suitable surface temperature measurement techniques on heated surfaces whilst exposed to external forced convection conditions was very limited (Liptak, 2002), not suitable for the required application, and/or was proprietary (Lamarsh and Barata, 2001). Thus, several methods (see Section 3) to measure surface temperature in the presence of the adjacent coolant had to be evaluated both experimentally and analytically to select the most appropriate one.

The methods and instruments employed to measure the surface temperature on both the Zr-4 and SiC clad-tubes had to be identical in order to claim the validity of the heat transfer results and to be able to make informed comparisons. In addition, it was essential that the selected surface measuring technique did not adversely affect the flow and thermal surface conditions. The ability to apply or remove the sensors without damaging or fouling of the clad-tube surface was another important consideration.

For the experimental testing, the clad-tube specimens were fitted with internally embedded and sealed electric cartridge-type heaters and then subjected to external forced convection flow conditions in an experimental test facility specifically designed and built for this purpose (Govinder et al., 2019). This facility is referred to as the University of Pretoria – Thermal-Hydraulic Flow-loop Cell (UP-THFC).

2. Experimental setup

2.1. Description of the UP-THFC

The UP-THFC facility was conceived with the primary purpose of conducting experimental heat transfer analysis on nuclear fuel clad-tubes in single and multiple pin arrays in super atmospheric conditions. This facility was designed to be capable of simulating the flow in most types of Light-Water nuclear Reactors (LWR) (albeit at much lower operating temperatures and pressures). It caters for atmospheric and super-atmospheric conditions for the heat transfer studies on the various clad-tube specimens and provides for either vertical upflow, vertical downflow, or horizontal flow conditions. A schematic of the flow loop is shown in Fig. 1.

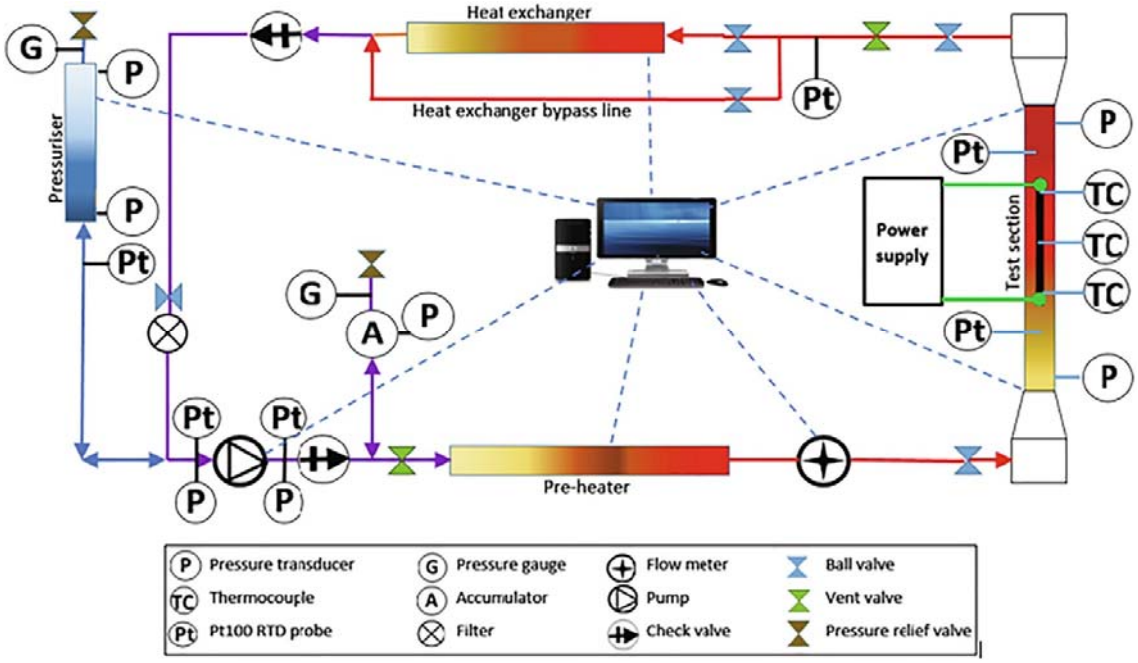

Fig. 1. Schematic representation of the UP-THFC experimental setup.

The flow direction through the test section is controlled via a valve-set that can be adjusted manually. A 7.5 kW centrifugal pump with a 40 m water-head capacity circulates the bulk water coolant through the flow loop. To damp-out pump induced pressure pulsations, a non-bladder type accumulator is installed downstream of the pump. Pre-heaters are located further downstream of the pump but ahead of a venturi flowmeter with a high precision differential pressure transducer. The test section duct is located between the flow meter and a heat exchanger. The heat exchanger provides an additional means to control the temperature of the water coolant before it re-enters the pump. A pressuriser allows for the manually adjusting static pressure head of up to 20 m to the suction side of the pump.

The 3 m long test section duct has an internal square profile of 80 mm × 80 mm. Plenum-boxes (headers) located on each end of the duct aids in the flow transition from the round 3-inch supply/discharge pipe network to the test section duct. Honeycomb type flow straighteners are incorporated in the plenum-boxes to reduce swirl and straighten the flow in the test section. The portion of the test section where the heated tubes (pins) are investigated, is located in the longitudinal centre of the duct and is designed to accommodate pin arrays of up to 550 mm heated length and up to a maximum 7 × 7 array of typical Zr-4 pins each with an outer diameter and pitch spacing of 9.5 mm and 11.43 mm respectively. This design can accommodate a 4 × 4 array of the presently available SiC tubes with an outer diameter and pitch spacing of 15.5 mm and 20 mm respectively. The test section is fitted with 500 mm × 50 mm observation windows (viewing portals) on three sides to cater for visual observations and videography of the boiling phenomena on the heated surfaces of the test specimens. Fig. 2 depicts the general cross-sectional schematic of the heated portion of the test section duct which shows a single fuel pin arrangement as well as the locations of the viewing portals.

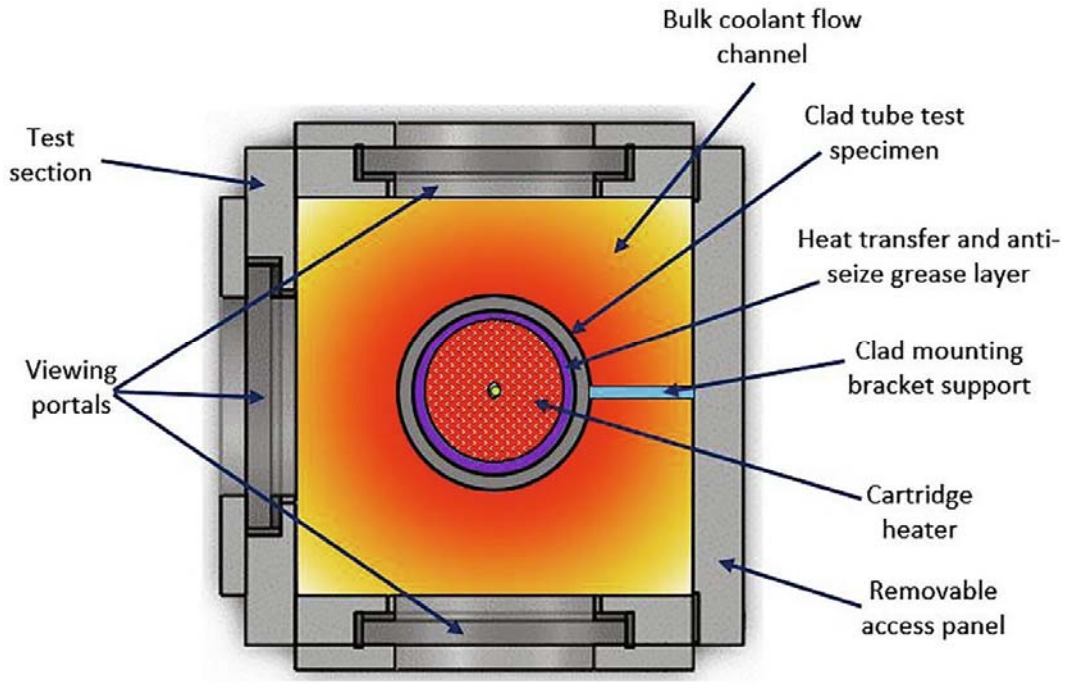

Fig. 2. Cross-sectional schematic (not to scale) of the UP-THFC test section depicting a single heated pin within the bulk coolant flow channel.

For access into the test section, the heated test section portion is equipped with a removable panel (access panel) as is depicted in Figs. 2 and 3. Additionally, the access panel serves as a mounting platform for the test specimen(s) and measuring instruments. This arrangement caters for the external pre-testing of the mounted clad-tube assembly in an auxiliary test tank to verify water tightness and equipment functionality prior to the access panel being installed on the test section.

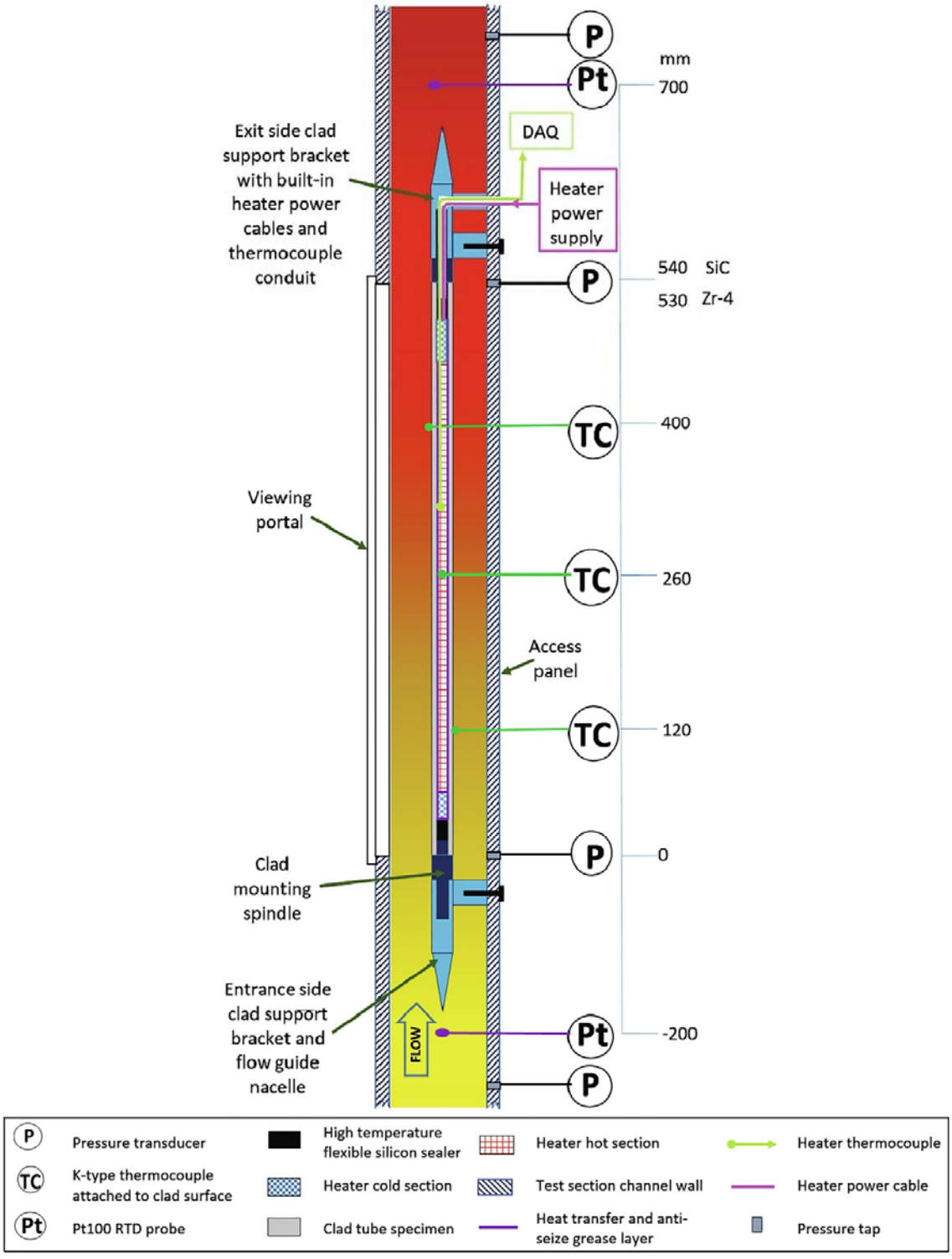

Fig. 3. Schematic of the heated portion of the UP-THFC test section showing a general longitudinal cross-sectional arrangement (not to scale) of a typical clad-tube test specimen mounted in place between support brackets. The locations and general layout of various test instruments are also indicated in the schematic.

The UP-THFC was fully built and operational in 2015. Verification and validation tests were then conducted to characterise the thermal–hydraulic flow regimes within the test section.

Whilst experiments and investigations were conducted in developing the clad surface temperature measuring technique, the flow loop was utilised for other research such as pressure drop experiments across tube bundles and spacer grids. In early 2019, the flow loop became fully operational for heat transfer experiments on various clad tubes once a suitable clad surface temperature measuring technique was established as detailed in Section 3. The operating specifications for the UP-THFC are as tabulated in Table 1. Uncertainties for the test instruments were established within the 95% confidence level and are tabulated in Table 2.

Table 1. Operating specifications for the UP-THFC.

Operating condition	**Location in the flow loop**	**Operating range/value**
Operating pressure	Test section	87 to 200 kPa (Abs.)
	Pump discharge port	400 kPa (Abs.)
	Pump inlet port	100 to 200 kPa (Abs.)
	Pressuriser	250 kPa (Abs.)
Design temperature	The inlet to test section	Ambient to 120 °C
*Design volumetric flow rate	System	100 to 975 L/min
*Mass flow rate	System	1.6 to 15.3 kg/s
Heated pin length	Test section	500 to 550 mm (typical)
Test section configuration	Test section	80 mm × 80 mm Square
Maximum pin array configurations	Test section	7 x7 Array of 9.5 mm Zr-4 Pins, or 4x4 Array of 15.5 mm SiC pins
*Flow velocities	Test section	Depends on pin array configuration and flow rate condition in the test section. Nominal 0.2 to 2.5 m/s.
	System pipeline	0.2 to 2.6 m/s

* Bulk water temperature-dependent.

Table 2. Test instrument uncertainties.

Instrument/Equipment	Range	Uncertainty
Thermocouples T-type	50 to 150 °C	0.1 °C
Pt100 RTD	95 to 150 °C	0.1 °C
Pressure transducers	0 to 250 kPa 0 to 1 000 kPa	0.025 kPa 0.1 kPa
Flow meter	2.5 to 11.5 kg/s	0.012 kg/s
Voltmeter	0 to 230 VAC	0.1 to 0.5 V
Ammeter	0 to 25 A	0.1 to 0.25 A

2.2. Experimental procedure

The experimental procedure for the testing of the adopted clad surface measuring experimental methods (as is discussed in Section 3), is described for the set-up for a single zircaloy-4 clad-tube specimen that was used in the tests in the present work but is readily applicable to the other measuring methods that are discussed in Section 3. The procedure starts with the test section of the flow loop drained and the access panel removed from the test section duct.

First, the cleaned outer surfaces of the cartridge heater and the inner surface of the clad tube were lubricated with a thermally conductive anti-seize paste and the heater inserted inside the bore of the specimen-clad tube. A high-temperature silicon-based sealing compound was filled into each end of the clad tube to seal the heater into the tube. The lead cables for the heater power and heater thermocouple were fed through the cable access provided on the exit side tube support bracket. Thereafter, the rod assembly was braced into position between the support brackets that were already fixed to the access panel Fig. 3. The thermocouples to measure the wall temperature were then fitted to the clad surface per the method mentioned in sub-section 3.4.

The assembled panel was then subjected to pre-testing of the test instruments and heater functionality in a separate purpose-built auxiliary tank. A test for a water tightness of the clad tube assembly and cable/instrument access points was also conducted in the auxiliary tank prior to fixing the assembled panel into the test section duct. The instrumentation signal output wiring was then routed into the data acquisition system and the cartridge heater was connected to a regulated power supply.

Prior to filling of the flow loop with the water, all drain valves were closed and all vent valves opened. In addition, all flow control valves in the pipe network were fully opened to prevent voids and air pockets from being created in dead legs of the pipe network. The water inventory was obtained from the building supply water but that which was first prepared by filtering for solids, heavy metals and added chemicals using reverse-osmosis technology. The prepared water was stored in a reservoir tank from which it was pumped through a deionising module and into the fill point located at the top of the pressurising unit. As the system filled, the air inside the pipes was vented through the vent valves, which were located at different elevation points on the flow loop. These valves were sequentially closed off manually when

the water bled out through each, observed through transparent pipes that directed the discharged water to auxiliary holding tanks. The system was completely filled when only water bled out from the vent valves at the highest points in the system located respectively on top of the pressurising unit and/or the test section assembly when orientated vertically.

The system was ready for testing when the flow loop was confirmed leak-free. The flow control valves were then set to attain the correct flow direction through the test section for the specific experiment. Thereafter, the pump and preheaters were powered on to commence the process of degassing of the water. After this procedure, which could take up to three days to complete, the required saturation pressure in the test section was set by manually adjusting the static pressure head of the pressuriser. The forced convective bulk water was then pre-heated to the required inlet water temperature. Around four hours was required to increase the water temperature from around 30 °C to 100 °C. A further two hours were required to get the temperature to 120 °C.

On attainment of the required bulk water inlet temperature, the system was then adjusted to the required test conditions for each experimental test point according to mass flow rate, test section pressure, bulk water inlet temperature, and cartridge heater power input. The system conditions were then allowed to attain a steady-state before testing commenced. Each incremental test parameter adjustment thereafter resulted in around two minutes for the system to settle and converge to the steady operational condition. A steady operational condition was defined as when at least five consecutively recorded data points showed negligible differences for the bulk water inlet temperature, pressure, and flow rate – as was observed via a bespoke computer-based graphical user interface, control module, and data acquisition system. The sequence of data logging commenced on achieving a steady operating condition. The physical test data was then recorded for the next 120 s. Following this, the next test point was set and a settling period of around 120 s (or more if necessary) was observed before commencing the next data logging event. The sequence was repeated until the required data set was recorded. Due to operational limitations of the data acquisition equipment, the data was recorded at a sampling frequency of around 0.4 Hz giving approximately 24 data points per minute.

Each complete test comprised of cycling through four pre-determined heat flux settings of the cartridge heater coupled with four different mass flow rates that amounted to 16 test conditions. At each mass flow rate, the heat flux was ramped up and down in sequence according to the four heat flux levels to provide one data set. For repeatability analysis, this sequence was repeated three times to provide three data sets per test condition. The data was recorded as described earlier above. A total of three completed tests was conducted for the adopted method (Section 3) and at least one complete test was conducted for the other methods. Due to the nature of the tests and the time required to set up the flow loop (excluding the time to install the test specimen and the degassing of the system), each complete test was conducted in a single sitting.

3. Techniques investigated to measure the external clad-tube surface temperatures

3.1. Non-contact surface temperature measuring methods

The use of pyrometers and infrared laser temperature measuring devices requires direct line-of-sight to the respective temperature emitting surfaces (Carlomagno and Cardone, 2010).

Although the observation windows in the test section cater to this, the effectiveness of these devices was shown to be incapable of measuring the actual surface temperatures while the surfaces were submerged in the surrounding water. The results showed clearly that the heated surfaces of the windows as well the heated convective bulk water flow within the test section produced a thermal barrier that in effect thermally obstructed the surface of which the temperature was to be measured.

The use of liquid crystal thermography methods (Cooper et al., 1975) was also not feasible since the coating could not be applied to surfaces that were directly exposed to the bulk coolant flow.

Non-contact surface temperature measuring methods was thus deemed impractical for this application and was abandoned.

3.2. Internally (non-wetted surface) mounted probes

It was reasoned that by measuring the inner clad-tube wall temperature, the external clad-tube wall temperature could be extrapolated analytically. This method thus required the location of temperature probes within the interface space between the heater and the inner clad-tube wall (air gap). Insulated thermocouples with a wire size of 36 to 40 AWG were used for this purpose. Experimental testing and analysis revealed that these internally mounted thermocouples were highly susceptible to electromagnetic interferences (EMI) that were emitted from the cartridge heater. The EMI effects produced erratic output temperature signals from the thermocouples which could not be used further for the heat transfer analysis. In addition, the temperature in the gap between the heater and the enveloping tube is very uncertain due to the uncertain nature of the thermal conductance in the dimensionless interface between two components. Extrapolation of this uncertain gap temperature to the outside surface gave virtually in all cases totally unreliable results and the method was subsequently abandoned.

3.3. Externally (wetted surface) mounted probes

This method entailed the attaching of temperature sensing probes directly onto the clad-tubes outer surface (wetted-surface).

Welding or brazing of probes onto the clad-tube surfaces (Flemons and Lane, 1971) was considered non-feasible, as this could not be achieved on the SiC surfaces. Clearly, this method would have also been further restrictive as the test probes would have been non-reusable or transferrable due to these being permanently attached to the respective clad-tube surface. This method also has the potential to cause a standing velocity and thermal boundary layer disturbance on the clad-tube surfaces. Subsequently, this method was not pursued further.

Sheathed temperature probes located and fixed at right angles (normal) to the heated surface were found to resemble cooling fins and provided temperature readings more closely related to the convective bulk water temperature than the actual clad-tube surface temperature. This method was therefore abandoned.

Axially (in-line) mounted sheathed probes could be physically clamped into place onto the clad-tube surface. At its point of application, these clamping components (such as mechanical

strapping, and, cable and wire ties) has the unavoidable potential of tripping (disturbing) the thermal and velocity boundary on the clad surface thereby, likely, changing the turbulence flow regime downstream of its location. Due to its low cost and ease of application, this method had potential and was developed further – as is discussed next.

3.4. The adopted surface temperature measuring technique

After considerable deliberation, it was thus an unavoidable option but to attach temperature probes on the outer surfaces of the clad-tubes. For these purposes, pre-calibrated K type sheathed thermocouples with a 0.75 mm outer diameter were selected. The sheathed thermocouples were routed via a compression gland through the access panel. An expansion loop was provided on the probe in order to compensate for thermal and strain effects. A length of approximately 25 mm of the sheathed probe, starting from its tip (sensor point), was attached axially onto the clad-tube. It was bound firmly onto the tube with 0.25 mm diameter stainless steel wire. Care was taken to locate the wire-ties from at least 10 mm downstream from the sensor tip to minimise disturbing the flow at the temperature measuring point. The general arrangement is shown schematically (not to scale) in Fig. 4.

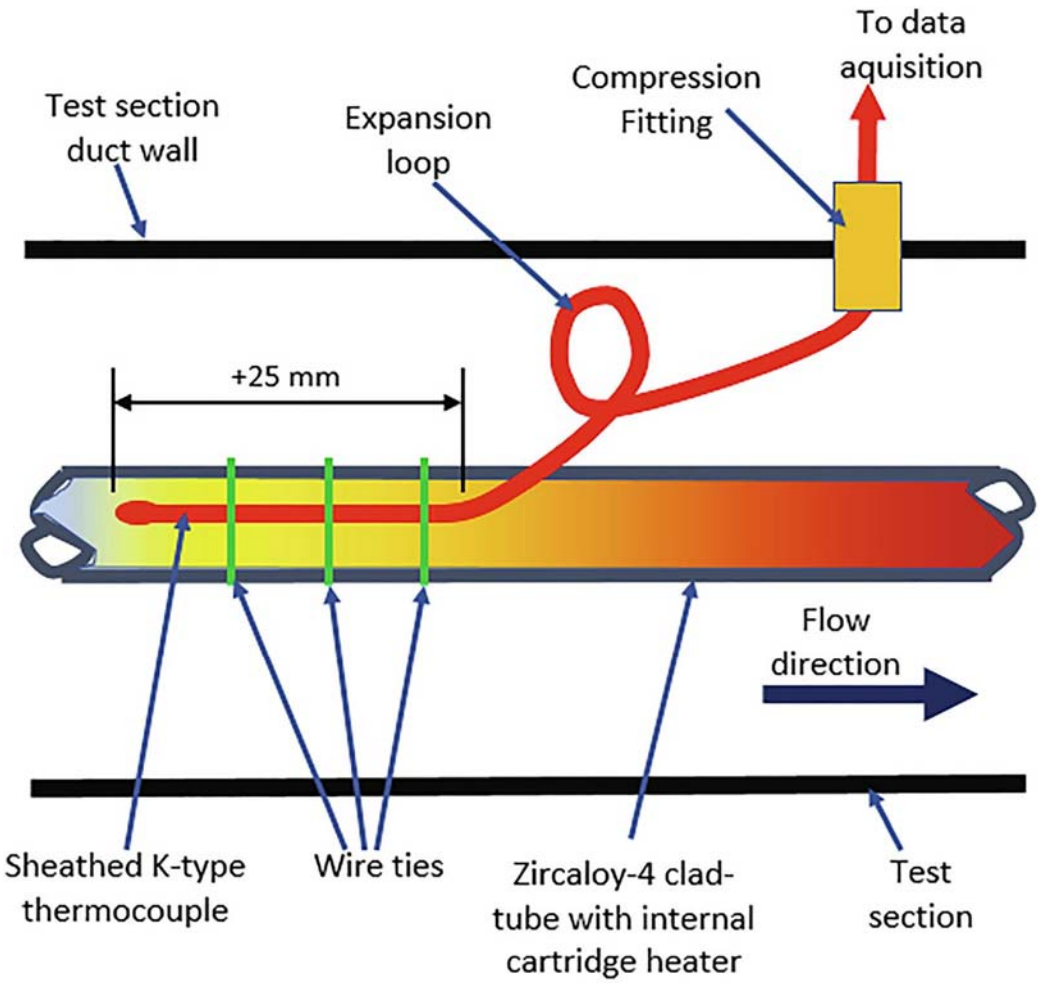

Fig. 4. Schematic of sheathed thermocouple fixed on zircaloy clad tube with stainless steel wire ties.

3.5. Abstract of techniques to measure the clad surface temperature

Table 3 provides a summary of the techniques investigated to measure the surface temperature on the heated clad tube. The advantages and disadvantages of each technique are highlighted and provide a brief insight as to how each compares with the adopted method. The adopted method itself is not a perfect solution but provides an acceptable means by which the clad surface temperature could be assessed.

Table 3. Comparison of measuring techniques.

Measurement Technique	Advantages	Disadvantages
Non-contact surface temperature measuring methods (pyrometers, infrared laser temperature measuring devices (FLIR), and liquid crystal thermography)	Ease of use within its respective operating capacity and capability. Certain FLIR camera models could capture both the video and photographic still thermal images of the surfaces under test.	Cannot measure the temperature of surfaces immersed and submerged within heated water. Required actual reference surface temperature/s for calibration purposes. Not feasible to apply liquid crystal thermography paint onto surfaces that were exposed to water as the water washed it off. Different coatings were required for different temperature ranges. Space limitations. The probe had to fit within the 0.1 mm air gap. Limited availability or scope for the miniaturization of probes for this scale magnitude.
Internally (non-wetted surface) mounted probes (thermocouples, thermistors)	Potential for the Inner clad wall temperature to be attained for centreline temperature analysis. The probe would not be in contact with the convective flow.	High potential for probe damage due to its exposure to very high temperature in the air gap due to the large uncertainty of the thermal conductance within the airgap. High potential for EMF interference when the probe is located alongside the electric resistance heaters The probe would not be in contact with the convective flow. Attaching or removing probes would require ingress into the test section.
Externally (wetted surface) mounted probes (welding/brazing/adhesives)	Welding of sheathed thermocouples on zircaloy clad tubes is existing and proven technology. The probe would be in	Not possible to weld/braze probes onto the ceramic SiC clad tubes. Suitable adhesives were not available at the time of the study. Difficult to remove probes without

Measurement Technique	Advantages	Disadvantages
	contact with the conducting heat transfer surface and the convective flow.	potential damage to both the probe and clad surface. The replacement clad materials and probes had a high-cost factor at the time of this study. Potential to disrupt the thermal and velocity boundary downstream of probe location. Attaching or removing probes would require ingress into the test section.
	The method can be applied to both the zircaloy and SiC clad tubes.	
Adopted surface temperature measuring technique (externally mounted probe secured onto the clad surface using wire ties)	Simple to attach or remove the probe. The process can be easily replicated. Cost-effective method. Probes and clad tube materials could be reused. The probe would be in contact with the conducting heat transfer surface.	Potential to disrupt the thermal and velocity boundary downstream of probe location. Attaching or removing probes would require ingress into the test section.

4. Data reduction

In this study, a single Zr-4 cladding-tube was utilised as the fuel pin specimen for the experimental testing. With the thermocouples installed on the surface as described in subsection 3.4, it was hypothesised that for the same set of measured temperatures and flow conditions in the flow loop, the experimental results could be interpreted in one of two ways:

1) The measured temperature(s) correlate the actual surface temperature:

$$T_{w,exp} = T_{meas} \tag{1}$$

2) The measured temperature(s) correlate the interface temperature (T_f) between the clad-tube surface and the bulk water stream. If the measured temperature is approximately the average between the surface temperature and the bulk water temperature then the surface temperature could, as a first approximation, be determined from:

$$T_{w,exp} = 2T_f - T_b \tag{2}$$

where,

$$T_b = \frac{T_{in}+T_{out}}{2} \tag{3}$$

To resolve the above conundrum, two methods were utilised for the evaluation of the surface measuring technique.

The first method made use of visual observations and videography techniques to identify the various boiling phenomena on the clad-tube surfaces by analysing the vapour bubble activity at various stages of the flow boiling activity (Cengel, 2006, Incropera and DeWitt, 1996, Collier and Thome, 1994). This involved the comparison of the input heat flux (q_{in}) to the boiling activity on the heated surface(s), and then comparing the observations to typical flow boiling processes as was described in the literature. According to the theory and descriptions in the literature, the start or onset of nucleate boiling phase (ONB) could be identified by the start of the formation of vapour bubbles on the heated surface. Typically, the ONB occur at an excess temperature (wall superheat) of about $\Delta T_{ex} = 5$ °C (Nukiyama, 1934). The was calculated using the following equation:

$$\Delta T_{ex} = T_w - T_{sat} \tag{4}$$

Upstream of the ONB point ($\Delta T_{ex} < 5$ °C), the single-phase forced convection is the dominant heat transfer mechanism. Downstream of the ONB point ($\Delta T_{ex} < 5$ °C), and dependant on the flow velocity and the wall superheat temperature, the vapour bubbles on the heater surface start to incrementally slide and coalesce along the heated surface leading to progressive lift-off of the vapour bubbles from the surface. The fully developed nucleate boiling phase (FDNB) occurs when the flow contains significant vapour void content or when the heated surface become fully obscured by the boiling activity (vapour generation) on the heated surface. The start of the FDNB is also referred to as the onset of significant void (OSV) (Dhir, 1991, Basu et al., 2003). The region between the ONB and FDNB is referred to as the partial nucleate boiling region (PNB). The boiling phenomena activity beyond the FDNB and up to the critical heat flux (CHF) region was not considered in the present study but is the subject of work to be conducted at a later stage.

The second method was to compare the experimental surface temperature results to that predicted with well recognised and accepted generalised forced convection boiling correlations. These correlations typically describe a combination of the macro-convective mechanisms associated with the flowing fluids (forced convection boiling) and the micro-convective mechanisms associated with vapour-bubble nucleation and growth (nucleate boiling) (Rohsenow, 1952).

Chen (1966) proposed the first widely recognised flow boiling heat transfer correlation for studies in vertical tubes. The Chen correlation included an additive mechanism to account for the micro- and macro-convective heat transfer to predict saturated flow boiling initially and later-on included subcooled flow boiling aspects. In Chen's equation, the modified Dittus and Boelter (1930) correlation was used for the liquid only forced convection heat transfer coefficient (h_l) and the Forster and Zuber (1955) correlation for the pool boiling component (h_{pool}).

Shah (1977) advanced a graphical method (*CHART*) for saturated boiling in which the convection coefficient (C_o) was introduced. Three other dimensionless parameters were defined for the use of this correlation and included the heat transfer enhancement factor (ψ), boiling number (B_o), and Froude number for liquid only phase (Fr_l).

Gungor and Winterton (1985) used a similar approach as that adopted by Chen (1966). Their correlation also included the enhancement and suppression factors for the saturated boiling heat transfer coefficient (HTC). The forced convection heat transfer coefficient (h_l) was the same as per the Dittus-Boelter equation (Dittus and Boelter, 1930) but the nucleate pool boiling heat transfer coefficient (h_{pool}) was per Cooper's (Cooper, 1984) correlation. A subsequent correlation by Gungor and Winterton (1987) was proposed to provide a more simplified model to determine the heat transfer coefficients for saturated boiling than their earlier work.

Kandlikar (1990) proposed a correlation refined from his earlier work (1983) that was suggested to be capable of predicting the heat transfer coefficient (h) versus the vapour quality (x) relationship. This correlation included familiar parameters such as h_l, C_o and B_o (that have been defined previously by Shah (1977) together with a published list of specific constants to be used respectively for forced convection and nucleate boiling regimes. Kandlikar stated that the h_{TP}/h_l factor in his correlation represented the larger yielded value for either the forced convection region or partial nucleate boiling region group of constants as determined by evaluation of the C_o value. Accordingly, the heat transfer in a convective boiling region dominated for the condition of $C_o > 0.65$. For $C_o < 0.65$, the nucleate boiling region dominated the heat transfer. Kandlikar thus suggested that this method provided continuity between the convective and nucleate boiling regions.

Liu and Winterton (1991) combined some of the concepts proposed by Kutateladze, 1931, Chen, 1966 in an effort to develop a generalised model to predict the flow boiling heat transfer coefficient. The authors proposed that the saturated heat transfer coefficient could be expressed as a combination of the single-phase forced convection heat transfer and the pool boiling heat transfer. Liu and Winterton claimed that their correlation could be used to accurately predict the surface temperature and clearly distinguish between nucleate boiling and forced convection effects. As such, the correlation was promoted to be used as a starting point in understanding the performance of surfaces designed to enhance heat transfer. The correlation was based on an explicit boiling term rather than an empirical boiling number dependence. Liu and Winterton have stated in their findings that other correlations that use the boiling number term B_o, prevents application to subcooled boiling analysis.

The correlations that were utilised in this study are listed in Table 4. In obtaining the predicted surface temperatures from these correlations, the heat transfer coefficient (h) was first determined using each correlation. The predicted surface temperature was then computed using the following equation:

$$T_{w,pred} = \frac{h}{\dot{q}_{in}} + T_b \tag{5}$$

Table 4. Forced convection boiling heat transfer correlations.

Chen (1966)	$h = Fh_L + Sh_{pool}$	$F = 1\left\{\frac{1}{X_{tt}} \le 0.1\right\}$ $F = 2.35\left\{\frac{1}{X_{tt}} > 0.1\right\}$	$S = \frac{1}{1+2.53\times10^{-6}\ Re_{TP}^{1.17}}$
Shah (1977)	$\psi = 230Bo^{0.5}$	$\psi = \frac{h}{h_L}$	$\psi = \frac{1.8}{Co^{0.8}}$
Gungor and Winterton (1985)	$h = Eh_L + Sh_{pool}$	$E = 1 + 24000Bo^{1.16} + 1.37(1/X_{tt})^{0.86}$	$S = \frac{1}{(1+1.15\times10^{-6}E^2Re_L^{1.17})}$
Gungor and Winterton (1987)	$h = (SS_2 + FF_2)h_L$	$F = 1.12\ (x/(1-x))^{0.75}\ (\rho_l/\rho_v)^{0.41}$ $F_2 = 1\ for\ vertical\ flow$	$S = 1 + 3000Bo^{0.86}$ $S_2 = 1 for vertical flow$
Kandlikar (1990)	$\frac{h}{h_L} = C_1Co^{C_2}(25Fr_{lo})^{C_5} + C_3Bo^{C_4}F_{fl}$		(see Rohsenow (1952) for values of constants (C_i))
Liu and Winterton (1991)	$h^2 = [Fh_l]^2 + [Sh_{pool}]^2$	$F = \left[1 + \mathrm{x}Pr_l\left(\frac{\rho_l}{\rho_v} - 1\right)\right]^{0.35}$	$S = \left[1 + 0.055F^{0.1}Re_l^{0.16}\right]^{-1}$
Dittus and Boelter (1930)	$h_L = 0.023Re_l^{0.8}Pr_l^{0.4}\left(\frac{k_l}{D_H}\right)$		(as used in Chen, 1966, Gungor and Winterton, 1985, Gungor and Winterton, 1987, Kandlikar, 1990, Liu and Winterton, 1991)
Cooper (1984)	$h_{pool} = 55p_r^{0.12}\dot{q}^{0.67}(-log_{10}\,p_r)^{-0.55}M^{-0.5}$		(as used in Gungor and Winterton, 1985, Gungor and Winterton, 1987, Kandlikar, 1990, Liu and Winterton, 1991)
Forster and Zuber (1955)	$h_{pool} = 0.00122\frac{k_l^{0.79}C_{pl}^{0.45}\rho_l^{0.49}(T_w-T_s)^{0.24}(P_w-P_s)^{0.75}}{\sigma^{0.5}\mu_l^{0.29}h_{fg}^{0.24}\rho_v^{0.24}}$		(as used in Chen (1966))

5. Results and analysis

5.1. Visual observations of the boiling phenomena

The flow boiling activity was visually observed and recorded for each experiment with the observations tabulated in Table 5. Average test section pressure was maintained at approximately 200 kPa. The Inlet pressure was equal to or more than the average saturated pressure in the test section to cater for the pressure drop across the test section. The testing

criteria included using four coolant mass flow rates in the test section together with four heater power settings. Generally, it was observable from the experiments that the level of visual boiling activity on the heated clad-tube surface decreased according to increasing mass flow rates when subjected to a heat flux. Instances of a few selected flow boiling activities are shown in the photographic plates in Fig. 5. As is discussed later in Section 6, the results from the visual observations are compared to the results from the surface temperature measuring analysis which is detailed in the following subsections.

Table 5. Summary of visual observed boiling activity at a bulk inlet temperature of 120 °C.

Flow Velocity [m/s]	Mass Flux [kg/m^2.s]	Heat Flux [kW/m^2] (Heater Power Input [kW])				Average Inlet Test Section Pressure [kPa]
		103.21 (0.86)	**142.40 (1.19)**	**191.46 (1.60)**	**236.94 (1.98)**	
0.25	**233.8**	PNB with numerous bubbles	Bubble sliding, coalescing and lift-off (OSV)	Mass bubbles coalescing and lifting-off (PNB)	Rapid ebullition (FDNB)	**198.7**
0.5	**476.8**	Small amount of bubbles forming	NB with numerous bubbles	Bubble sliding, coalescing and lift-off (OSV)	Mass bubbles coalescing and lifting-off (PNB)	**205**
0.75	**716.5**	No Bubble activity	Small amount of bubbles forming	ONB with bubbles lift-off but no coalescing	Bubble sliding, coalescing and lift-off (OSV)	**208**
1	**957.5**	No Bubble activity	No bubble activity	No bubble activity	Slight ONB activity	**213**

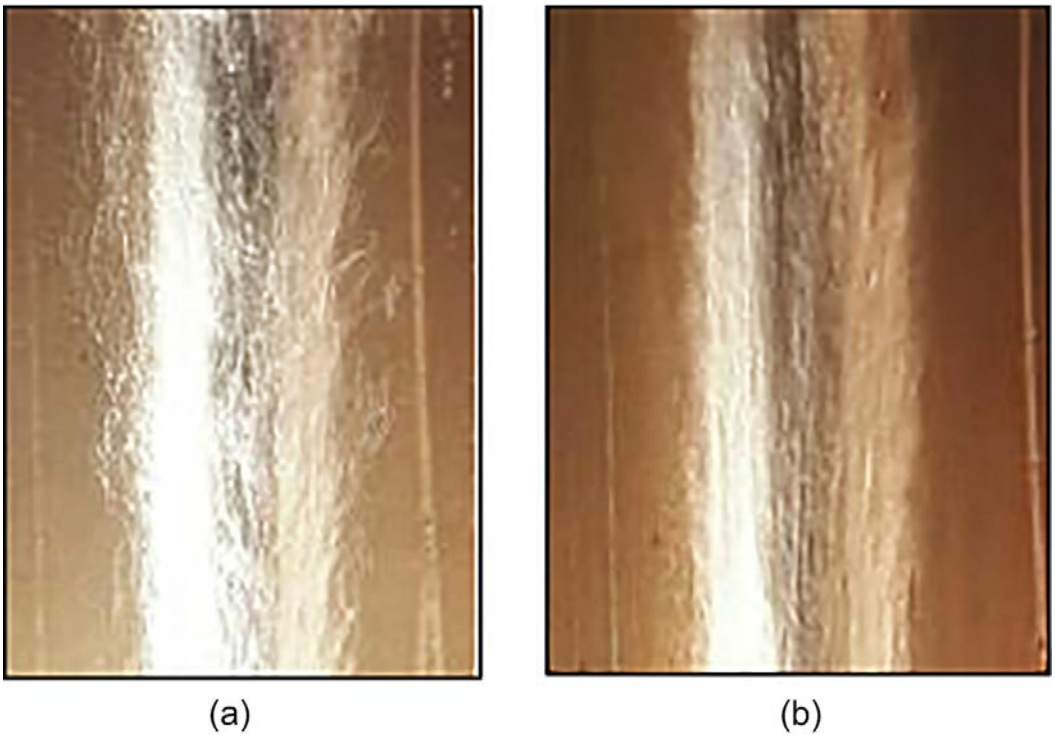

Fig. 5. Flow boiling phenomena at T_{in} = 120 °C, heat flux of 236.9 kW/m^2, and flow velocities in the test section at (a) 0.25 m/s, and (b) 0.5 m/s.

5.2. Results of measured temperature values that were correlated as actual surface temperatures

The results from the analysis of the data for this case are presented in the boiling curves in Fig. 6. These curves are indicative of typical flow boiling heat transfer trends. The outcomes for this case show that with increasing heat flux, the wall temperatures increase accordingly. The boiling curves also follow predictable behaviour which shows that at a heat flux, the heat transfer associated with the lowest flow rates produces the largest wall superheat values. To ascertain the level of rationality of these experimental results, a comparison was conducted between the experimentally measured values against predicted values that were computed from the various flow boiling correlations (Table 4). The results of the findings are presented graphically in Fig. 7. For this study case it is quite evident, according to this comparison, that all the results using the correlations to predict the surface temperature significantly over-predicts the wall temperature as compared to the corresponding experimentally measured values.

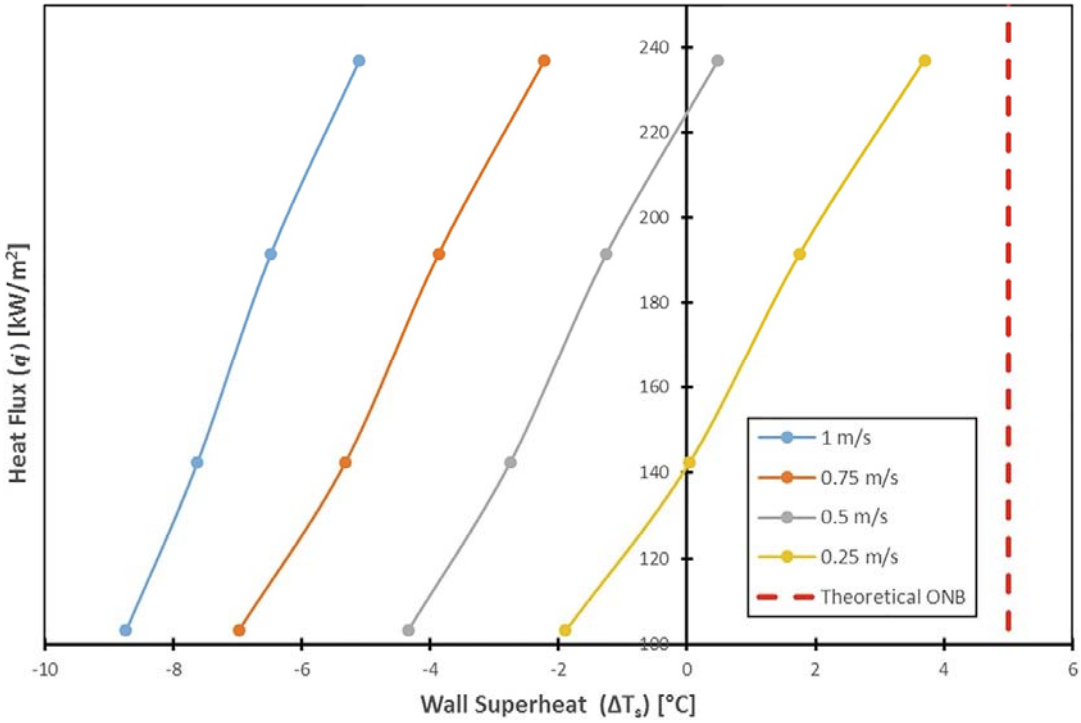

Fig. 6. Boiling curves for measured temperature correlated as actual surface temperature.

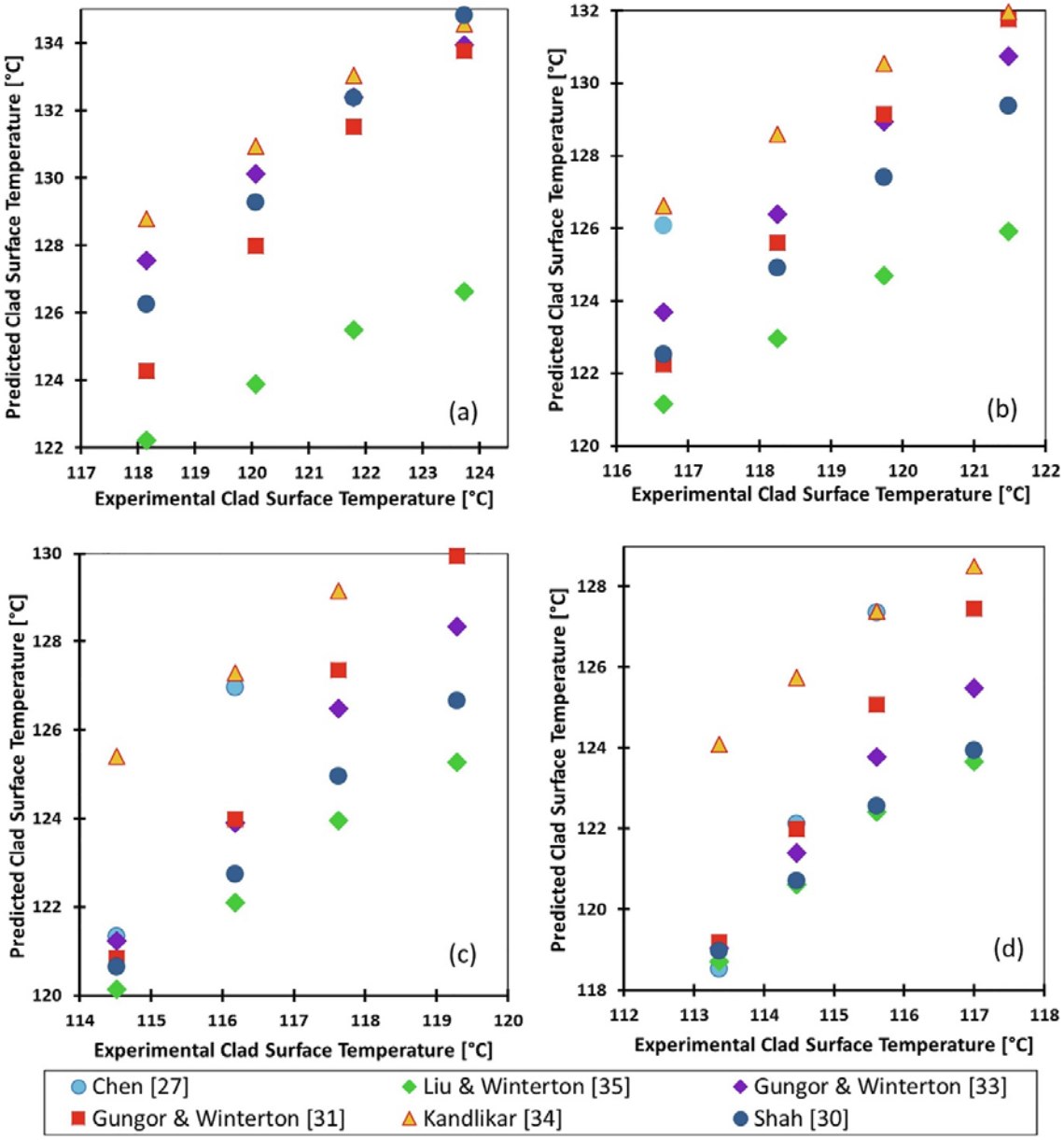

Fig. 7. Comparison of experimental and predicted wall surface temperature for the case of measured temperature correlated as actual surface temperature for test section flow velocities at (a) 0.25 m/s, (b) 0.5 m/s, (c) 0.75 m/s, and (d) 1 m/s.

5.3. Results for measured temperature values that were correlated as equivalent interface temperatures

In this case, the wall surface temperature, and hence the wall superheat, was calculated using Eqs. (3), (4). The yielded results are presented graphically in Fig. 8. The results obtained in this case follows typical flow boiling trends for such boiling activity and flow conditions. However, for the same heat flux and bulk coolant flow conditions, the results now show significantly higher wall superheat values than that obtained in the previous case. This outcome was further augmented by the comparisons between the experimental and predicted surface temperatures that are presented in Fig. 9 in which the solid line indicates the line of

best fit and the dashed lines being indicative of the upper and lower confidence bands respectively which corresponds to a 95% confidence interval. The increasingly under-predicted wall temperature at increasing heat flux could be attributed to changes in the interface layer thickness due to higher or more energetic bubble activity. The presence of the thermocouple within this thickness and its influence thereof still needs investigation. No tip lift-off or the formation of a stagnation void was detected during observations when the thermocouple was not obscured by bubble activity. The investigations of these latter aspects were beyond the scope of the current work and will be subjected to future investigations.

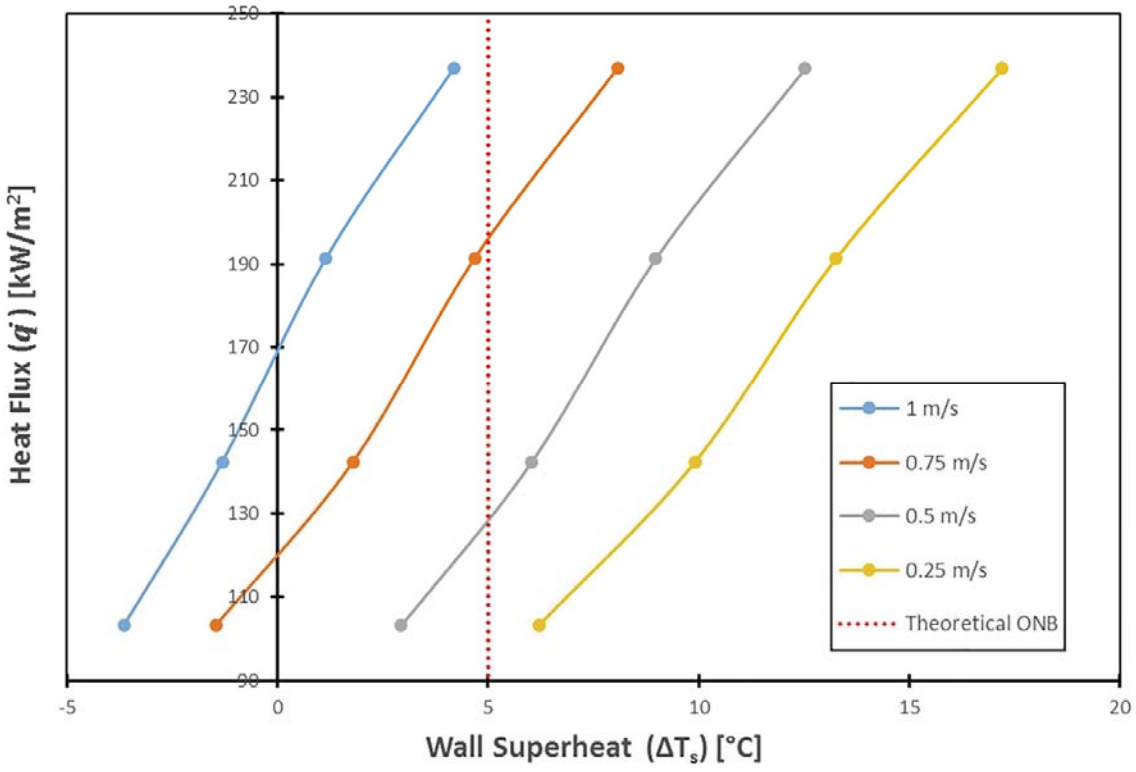

Fig. 8. Boiling curves for measured temperature correlated as a film or interface temperature.

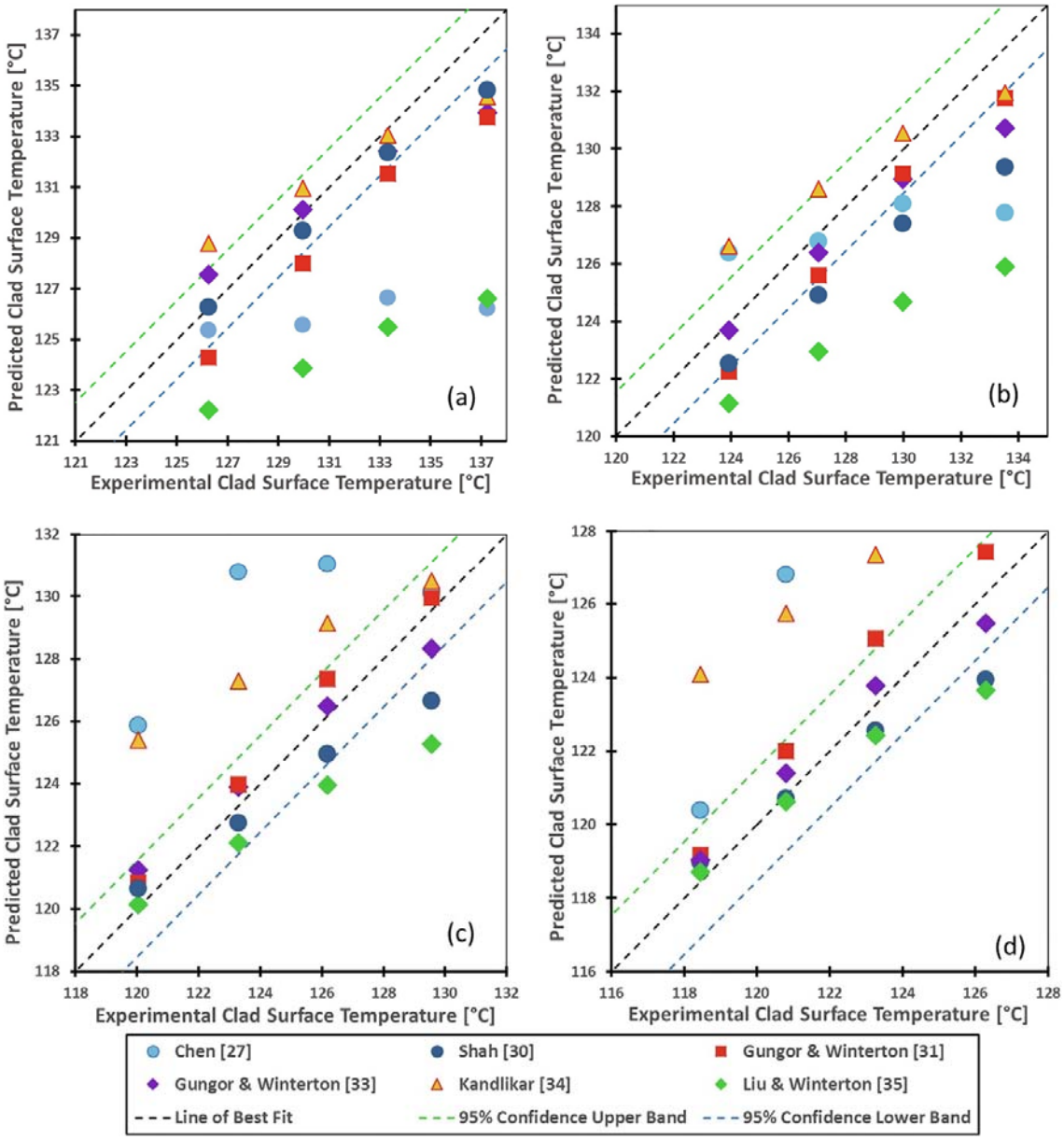

Fig. 9. Comparison of experimental and predicted wall temperature for the case of measured temperature correlated as a film or interface temperature. The dashed line indicates the line of best-fit.

Overall, the results for this case show much closer agreement between the experimental and predicted surface temperature for certain ranges of correlated values than was achieved with the previous case.

6. Discussion of results

From the analysis of the two hypotheses (as detailed above), it is evident that the measured surface temperature that was correlated as that of the interface temperature from which the wall temperature was subsequently determined, was the most acceptable approach. The resultant outcomes from this finding relate well with the visual observations shown in the photographic plates in Fig. 5 and the observed boiling activity descriptions in Table 5. This

assessment is also supported by the relatively good agreement between the experimental results with the predicted results – particularly from the two significantly different Gungor-Winterton correlations (Gungor and Winterton, 1985) (Gungor and Winterton, 1987). Most of the results that were predicted by these correlations in conjunction with the adopted measuring technique, showed much closer agreement with experimental results than was ever achieved by the other clad surface temperature techniques – as was discussed earlier in Section 3. Overall, none of the correlations could predict values that could exactly mimic the experimental values. A possible reason could be the generalisation of these correlations for application with a wide range of heat transfer liquid mediums.

The repeatability analysis of the tests with the same conditions yielded averaged results between 0.4 and 0.9 °C which was within the uncertainty range of the instrument (1.5 °C). The estimated uncertainties of the various measured and calculated heat transfer related values are tabulated in Table 6. The uncertainty analysis follows the procedures set out by Moffat, 1988, Dunn, 2010 for a 95% confidence level. Generally, the uncertainty of the heat flux was found to decrease with increasing heat flux levels due to the higher stability of the SSR power regulator at the higher power (heat flux) settings than at the lower power settings. Although different SSRs of the same model type were tested, these all produced the same outcomes. At this stage, it is still unknown as to why the SSR behaved less stable at the low heat flux settings and this warrants further future investigation into this matter.

Table 6. Uncertainty of measured and calculated values during dynamic conditions.

Parameter	Uncertainty
Minimum heat flux	±1.8% at 25 kW/m^2
Maximum heat flux	±0.3% at 195 kW/m^2
Saturation temperature	±0.1 °C ± 0.5%
Clad Wall Surface temperature	±1.5 °C ± 0.5%

The test results obtained using the adopted surface temperature measuring technique has catered for a better understanding of the heat transfer testing capacity and capability of the UP-THFC.

7. Conclusion

Extensive experimental investigations have been undertaken in the UP-THFC to determine an appropriate method to measure the external surface temperature on internally heated clad-tubes when these are exposed to external forced convection flow boiling conditions. The technique that was developed and adopted uses axially aligned sheathed thermocouple probes positioned and fastened by wire ties onto the external heated surface portions of the clad tube. The findings from this study have established that the hypothesis that relates the measured temperature to that of the interface temperature that which represented the average temperature value between the clad surface and the bulk flow has been found to be a feasible approach. The average value was used as a first approximation and the results obtained from this provided a reasonably good fit between observed interpretations of the boiling phenomena on the clad surface as well as with the prevailing boiling theory (Collier and

Thome, 1994, Nukiyama, 1934). Since this is a novel approach in acquiring knowledge of this complex heat transfer mechanism, further work would be required to ascertain whether this technique could be utilised for the prediction of the size and temperature of the interface layer. This result thus provides a basis from which further comparative heat transfer testing on the various fuel clad-tube specimens can proceed in the UP-THFC.

Most of the correlations that were utilised in this study were mainly derived for internal forced convection flow boiling conditions in externally heated tubes. The results in this study thus also establish that these correlations can be successfully applied to external heat transfer from internally heated tubes.

CRediT authorship contribution statement

K. Govinder: Methodology, Investigation, Validation, Visualization, Writing - original draft. **J.F.M. Slabber:** Supervision. **J.P. Meyer:** Supervision.

Declaration of Competing Interest

The authors declare that they have no known competing financial interests or personal relationships that could have appeared to influence the work reported in this paper.

Acknowledgements

• Funding for the project was obtained from the Institutional Research Theme (IRT) on Energy at the University of Pretoria.

• This work has been supported and also partially funded by the Clean Energy Research Group (CERG) in the Department of Mechanical and Aeronautical Engineering at the University of Pretoria, South Africa.

• Endress + Hauser South Africa donated a high precision differential pressure transducer and also provided (gratis) calibration of the flow meter.

• H. Kampmann and Co. donated the secondary and tertiary pumps.

• Hydrax, South Africa donated the coolant reservoir and water make-up tanks.

References

Accident-Tolerant Fuel Valuation: Safety and Economic Benefits (Revision 1) 3002015091," Electric Power Research Institute (EPRI), 22 March 2019. [Online]. Available: https://www.epri.com/#/pages/product/3002015091/?lang=en-US. [Accessed 15 November 2019].

Anglart, H. "Applied Reactor Technology," 2011. [Online]. Available: http://www.diva-portal.org/smash/get/diva2:500610/fulltext01.pdf.

Basu, N., Warrier, G., Dhir, V., 2003. Wall Heat Flux Partitioning During Subcooled Flow Boiling at Low Pressures. Proceedings of HT2003 - ASME Summer Heat Transfer Conference. Las Vegas, Nevada, USA.

Buongiorno, J., 2011. Technical Lessons Learned from the Fukushima-Daichi Accident and Possible Corrective Actions for the Nuclear Industry: An Initial Evaluation, Center for Advanced Nuclear Energy Systems, MIT-NSP-TR-025, May 2011.

Carlomagno, G., Cardone, G., 2010. Infrared thermography for convective heat transfer measurements. Exp. Fluids 49, 1187–1218.

Carpenter, D., Ahn, K., Kao, S., Hejzlar, P., Kazimi, M., 2007. Assessment of Silicon Carbide Cladding for High-Performance Light Water Reactor, Nuclear Fuel Cycle Program, Vol. MIT-NFC-TR-098, 2007.

Cengel, Y., 2006. Heat and Mass Transfer: A Practical Approach, 3rd ed. McGraw-Hill, New York.

Chen, J.C., 1966. Correlation of Boiling Heat Transfer to Saturated Fluids in Convective Flow. I&EC Process Des. Dev. 5 (3), 322–329.

Collier, J., Thome, J., 1994. Convection Boiling and Condensation, 3rd ed. Clarendon Press, Oxford.

Cooper, M., 1984. Saturation Nucleate Boiling. A Simple Correlation. 1st UK National Conference on Heat Transfer.

Cooper, T., Field, R., Meyer, J., 1975. Liquid Crystal Thermography and Its Application to the Study of Convective Heat Transfer. Heat Transfer 97 (3), 442–450.

Dhir, V., 1991. Nucleate and Transition Boiling Heat Transfer Under Pool and External Flow Conditions. Int. J. Heat Fluid Flow 12 (4), 290–314.

Dittus, F., Boelter, M., 1930. Heat Transfer in Automobile Radiators of the Tubular Type. University of California Publications on Engineering 2, 433–461.

Dunn, P., 2010. Measurement and Data Analysis for Engineering and Science. CRC Press, Boca Raton.

Feinroth, H., Ales, M., Barringer, E., Kohse, G., Carpenter, D., Jaramillo, R., 2009. Mechanical Strength of CTP Triplex SiC Fuel Clad Tubes After Irradiation in MIT Research Reactor under PWR Coolant Conditions. The 33rd International Conference on Advanced Ceramics and Composites.

Flemons, R., Lane, A., 1971. Thermocouples for surface temperature measurement in multielement nuclear fuel bundles, in Fifth Symposium on Temperature, Washington DC.

Forster, H., Zuber, N., 1955. Dynamics of Vapor Bubbles and Boiling Heat Transfer. J. Am. Inst. Chem. Eng. (AIChE) 1 (4), 531–535.

“Fukushima Daiichi Accident,” World Nuclear Association, [Online]. Available: https:// www.world-nuclear.org/information-library/safety-and-security/safety-of-plants/ fukushima-daiichi-accident.aspx. [Accessed 20 April 2020].

Govinder, K., Slabber, J., Meyer, J., 2019. Theoretical Analysis and the Design, Construction and testing of a Flow Loop for the Study of Generalized Forced and Natural Convection Boiling Heat Transfer Phenomena on Typical Light Water Nuclear Reactor Fuel Pin Configurations. University of Pretoria, Pretoria, South Africa.

Gungor, K., Winterton, R., 1985. A General Correlation for Flow Boiling in Tubes and Annuli. Int. J. Heat Mass Transf. 29 (3), 351–358.

Gungor, K., Winterton, R., 1987. Simplified General Correlation for Saturated Flow Boiling and Comparison with Data. Chem. Eng. Res. Des. 65 (2), 148–156.

Gurgen, A., Shirvan, K., 2018. Estimation of coping time in pressurized water reactors for near term accident tolerant fuel claddings. Nucl. Eng. Des. 337, 38–50.

Incropera, F., DeWitt, D., 1996. Introduction to Heat Transfer. John Wiley & Sons, New York, USA.

Kandlikar, S., 1990. A General Correlation for Saturated Two-Phase Flow Boiling Heat Transfer Inside Horizontal and Vertical Tubes. J. Heat Transfer 112, 219–228.

Kutateladze, S., 1931. Boiling Heat Transfer. Int. J. Heat Mass. Lamarsh, J., Barata, A., 2001. Introduction to Nuclear Engineering, 3rd Edition, New Jersey. Prentice-Hall, USA.

Lee, Y., McKrell, T., Kazim, M., Key Structural Challenges for SiC as Fuel Cladding for LWRs, in Proceedings of ICAPP, Charlotte, USA, 2014, April 6-9.

Liptak, B.G., et al., 2002. Instrument Engineers Handbook, 3rd ed. CRC Press.

Liu, Z., Winterton, R., 1991. A General Correlation for Saturated and Subcooled Flow Boiling in Tubes and Annuli, Based on a Nucleate Pool Boiling Equation. Int. J. Heat Mass Transf. 34 (11), 2759–2766.

McMinn, A., Darby, E.C., Schofield, J.S., 1998. The Terminal Solubility of Hydrogen in Zirconium Alloys. 12th International Symposium on Zr in the Nuclear Industry, Toronto.

Moffat, R., 1988. Describing the Uncertainties in Experimental Results. Exp. Therm Fluid Sci. 1 (1), 3–17.

Nechaev, A. Corrosion of Zirconium Alloys in Nuclear Power Plants, IAEA-TECDOC-684, p. www.iaea.com, 1993.

Nishio, S., 2004. Fusion Power Reactor Designs Adopting SiC/SiC Composite as the Structural Material. J. Plasma Sci. Nucl. Fusion Res. 80 (80), 1–14.

Nukiyama, S., 1934. The Maximum and Minimum Values of the Heat Q Transmitted from Metal to Boiling Water under Atmospheric Pressure. J. Jpn. Soc. Mech. Eng. 37, 367–374.

Rohsenow, W., 1952. A Method of Correlating Heat Transfer Data for Surface Boiling Liquids. Trans. ASME 74, 969–976.

Shah, M., 1977. A General Correlation for Heat Transfer During Subcooled Boiling in Pipes and Annuli. ASHRAE Trans. 83, 205–215.

Sukjai, Y., Shirvan, K., Pilat, E., Kazimi, M., 2014. The effects of SiC cladding thickness on advanced PWR fuel rod performance, in Proceedings of ICAPP 2014, Charlotte, USA, 2014, April 6-9.

Voglewede, J., 2012. Nuclear Fuel Safety Criteria Technical Review, 2nd Edition, Organisation for Economic Co-operation and Development (OECD); Nuclear Energy Agency (NEA).